

A study on mass transfer modelling in SOFC anode: Comparison of diffusion mass transfer models for estimation of diffusion overpotential

P. Ramakrishnan* , Abanti Sahoo 

NIT Rourkela, Department of Chemical Engineering, Rourkela, Sector-1, Sundergarh, Odisha, India, 769008

* Corresponding author:

e-mail:

p_ramakrishnan@nitrkl.ac.in
p.ramakrishnan9@gmail.com

Article info:

Received: 31 October 2022

Revised: 25 January 2023

Accepted: 06 March 2023

Abstract

The mathematical approach to SOFC modelling helps to reduce dependence on the experimental approach. In the current study, six different diffusion mass transfer models were compared to more accurately predict the process behavior of fuel and product diffusion for SOFC anode. The prediction accuracy of the models was extensively studied over a range of parameters. New models were included as compared to previous studies. The Knudsen diffusion phenomenon was considered in all the models. The stoichiometric flux ratio approach was used. All the models were validated against experimental data for a binary (CO–CO₂) and a ternary fuel system (H₂–H₂O–Ar). For ternary system, the pressure gradient is important for pore radius below 0.6 μm and current density above 0.5 A/cm². For binary system, the pressure gradient may be ignored. The analysis indicates that the MBFM is identified to be the best performing and versatile model under critical SOFC operating conditions such as fuel composition and cell temperature. The diffusive slip phenomenon included in MBFM is useful in SOFC operating conditions when fuel contains heavy molecules. The DGMFM is a good approximation of DGM for the binary system.

Keywords

Solid Oxide Fuel Cell, Knudsen diffusion, diffusion overpotential, pressure gradient, tortuosity factor

1. INTRODUCTION

The Solid Oxide Fuel Cell (SOFC) is a complex solid-state electrochemical energy conversion device consisting of solid-solid and gas-solid interfaces. A planer SOFC consists of an electrolyte in between two electrodes, namely anode and cathode. It converts chemical energy stored in fuel into electrical energy via electrochemical combustion at high temperatures ranging between 500–1000 °C (Jacobson, 2010). The SOFC technology is considered to be an eco-friendly, sustainable and versatile energy conversion method. Moreover, it may be considered as an indirect renewable energy source (Abdalla et al., 2018). The SOFC can produce electricity with an energy conversion efficiency of approximately 60% (Shaikh et al., 2015). The ability of SOFC to utilize carbon containing fuels such as natural gas, biogas, alcohol, gasoline, methanol, etc. followed by the efficiency advantage suggests that the SOFC may be a part of future technologies (Shaikh et al., 2015; Zhou et al., 2016). Nowadays, the research related to SOFC is mainly focused on operating temperature reduction, component materials' catalytic activity enhancement and device structure optimization. The objectives are to maximize the rate of energy conversion, energy efficiency and stability.

Among various proposed cell structures, anode supported designs are able to offer higher current density and long term stability (Bao et al., 2016). The binary diffusion coefficient value of H₂–H₂O is found to be about four times that of

O₂–N₂ (Singhal and Kendall, 2003). Therefore, anode supported cell designs are preferred to reduce diffusion overpotential. The electrolyte used in SOFC is made thinner to reduce ohmic loss and cell operating temperature. A thick electrode is used to bear the mechanical stress of the cell. At the same time, the rate of mass transfer in electrode declines with the increase in electrode thickness leading to increase in diffusion overpotential and further loss in cell efficiency. The typical thickness of the anode in an anode supported cell is around 500–1000 μm. For cathode and electrolyte in an anode supported cell, the typical thickness is less than 50 μm (Bove and Ubertini, 2008). As a result, the diffusion overpotential of electrolyte and cathode is much less compared to anode due to their low thickness. In literature, numerous mathematical models have been proposed to best describe gaseous diffusion phenomena in the SOFC. These complex models are supposed to help optimize cell design by tuning the variables such as anode layer thickness, pore diameter and tortuosity at operating temperature and fuel concentration. In this work, various models are evaluated to determine the most accurate and versatile model under SOFC operating conditions. All of the models considered in this article consider two types of diffusion namely, molecular and Knudsen diffusion which are common to the porous medium of an anode electrode. The molecular diffusion considers molecule-molecule interactions. The Knudsen diffusion considers wall-molecule interaction. The SOFC has a typical pore diameter of 2 μm in anode support material and 1 μm in the anode catalyst layer. The molecular mean free path of 0.1–1 μm



is typical for SOFC. The Knudsen number is defined as the ratio of molecular mean free path and characteristic length of medium (e.g. pore diameter). For SOFC, its typical value may fall in slip ($0.001 < Kn < 0.1$) or transition region ($0.1 < Kn < 10$) (Haberman and Young, 2006). Therefore, it is essential to include both molecular and Knudsen diffusion to best describe mass transfer phenomena in SOFC.

The Fickian model (FM) is the simplest approach found in the literature to describe mass transfer phenomena in SOFC. However, it considers only one-way interaction of the molecules (Pant et al., 2013). A Modified Fickian model (MFM) may be obtained by using the effective Fickian diffusion coefficient in the standard or extended model (Bao et al., 2016). Another way to obtain a differently modified form of Fickian model is to include the effects of surface diffusion using exponential weighted average (Błesznowski et al., 2022; Gholaminezhad et al., 2017). However, a major drawback of this method surfaces when the activation energy of adsorption and surface diffusion coefficients are applied as fitting parameters. This renders the modelling results applicable to a particular reaction only (Błesznowski et al., 2022). The Stefan–Maxwell model (SMM) is easy to apply and overcomes the limitation of the FM. Nevertheless, it considers only molecular diffusion and ignores the Knudsen diffusion. The extended Stefan–Maxwell model (eSMM) considers the Knudsen diffusion by empirically improving the binary diffusion coefficient in SMM (Bao et al., 2016). The Dusty Gas model (DGM) adds a Knudsen diffusion term and Darcy's viscous flux term to the SMM. The literature survey insisted on including the Knudsen diffusion mechanism for SOFC electrodes. Preferably, the DGM is capable of doing so without any major observable limitations (Błesznowski et al., 2022). Currently, this is the model of choice for SOFC related studies. Numerous computational fluid dynamics (CFD) analysis was conducted for SOFC mass transport incorporating the DGM (Błesznowski et al., 2022). However, the pressure gradient term is often ignored to simplify implementations at the cost of accuracy. Kong et al. (2012) modified the DGM in form of the FM (DGMFM) to make DGM more user-friendly. The DGMFM can calculate molar flux independently if gas properties and distribution are provided. However, the scientific accuracy of the DGM for a multi-component system was questioned in the past works (Kerkhof, 1996; Wang et al., 2012). A study by Kerkhof (Kerkhof, 1996; Vural et al., 2010) argued that the DGM double counted the viscous term and went on to develop the Binary Friction model (BFM). The BFM can also reproduce Darcy's law based pressure drop equation when summed over all the components, just like the DGM (Zhu and Kee, 2003). Darcy's equation used in DGM and BFM assumes a no-slip boundary condition at the wall (Pant et al., 2013). However, in the literature, it has been shown that the diffusion slip may exist for multicomponent mixture flows (Pant et al., 2013). The no-slip assumption may introduce an error in estimation when used with the multi-component mixtures. Therefore, Pant et al. (2013)

modified Binary Friction model (MBFM) to account for diffusion slip and estimated viscous flow in pore by the Poiseuille approximation. Some of the models described here were compared by authors. Błesznowski et al. (2022) and Cayan et al. (2009) compared the FM and SMM and observed an increase in difference between the models at higher current densities. Suwanwarangkul et al. (2003) compared a modified FM, SMM and DGM for fuel product mixture containing binary CO–CO₂ and ternary H₂–H₂O–Ar components. The results were compared with experimental data of Yakabe et al. (2000) for an anode-supported SOFC in the planar configuration. They concluded the DGM to be most accurate at small pore size and low reactant concentrations. The SMM was found to be useful at high reactant concentration and low operating current density. However, the pressure gradient across the anode was ignored. Moreover, the mole fraction of Ar was assumed to be constant in the mixture. This is not true because a change in concentration of other components will cause a change in concentration of Ar (Vural et al., 2010). Vural et al. (2010) did a similar study with varied tortuosity factor. Although, the BFM is fitted with a larger tortuosity factor and pore size was interpreted as pore radius. Therefore, the results obtained from this study may be inaccurate. Bao et al. (2016) compared MFM, SMM, eSMM and DGM with different flux ratio approaches. The stoichiometric approach was found to be superior as the Graham approach ignores the pressure gradient across the anode. Wang et al. (2012) surveyed the multicomponent models namely DGM, BFM and Cylindrical pore interpolation model (CPIM). The study included methane-fed SOFC along with binary CO–CO₂ and ternary H₂–H₂O–Ar systems. The tortuosity squared is used as tortuosity factor in that study with an explanation that the square appears twice due to the gradient and the void volume associated with porosity (Mason and Malinauskas, 1983; Wang et al., 2012). The experimental works predicting the SOFC anode tortuosity factor to be in the range of 1.5 to 2 were also cited by the authors. Błesznowski et al. (2022) have performed a unique study on mass transport in SOFC electrode. The numerical analysis performed using a model implemented in Ansys Fluent revealed various factors contributing to the diffusion overpotential. The molecules having smaller Knudsen diffusion coefficient were found to be more likely to affect the cell voltage. The pressure gradient did contribute insignificantly to the total mass transport in SOFC. The CFD study was able to determine an ideal mean resident time for diffusing species. All the studies carried out so far do not include modifications made to DGM and BFM. Moreover, the difference between the DGM and MBFM results needs to be studied. The results obtained from DGMFM should also be compared to other models over a wide range of operating parameters. Hence, an attempt has been made in the present work to compare the models considering both types of diffusion except the CPIM. It is understood that the CPIM is rarely used for SOFC related studies (Wang et al., 2012). The importance of Knudsen diffusion for H₂ transport in SOFC was expounded by Yang et al. (2016)

and Błesznowski et al. (2022). Therefore, all the models considered in the study include a term to account for Knudsen diffusion. The stoichiometric approach is used in this study as the Graham approach ignores the pressure gradient across anode. The pressure gradient is considered and the tortuosity factor is fitted to compare diffusion overpotential predictability of the models. The effects of pore radius and pressure gradient are discussed later on.

2. MODEL DEVELOPMENT

A unit cell SOFC comprises two porous electrodes separated by a thin electrolyte layer. For an anode supported SOFC the thicker and porous anode layer is typically made of an ion-electron conduction mixture. The fuel is fed to the anode channel and air comes in from the cathode channel as illustrated in Figure 1. The fuel H₂ or CO move towards the anode electrolyte (A/E) interface via a diffusion mechanism. At the A/E interface, the fuel is oxidized to produce H₂O or CO₂. The electrons go through an external circuit to complete the circuit and generate a usable electric current. The products move away from the A/E interface towards the anode channel (A/C) interface and eventually go out through the anode channel outlet. The A/E and C/E interface should not be confused with triple phase boundary (TPB) as for perovskite anodes the TPB can spread throughout the anode. In Figure 1 the TPB is limited to interfaces only.

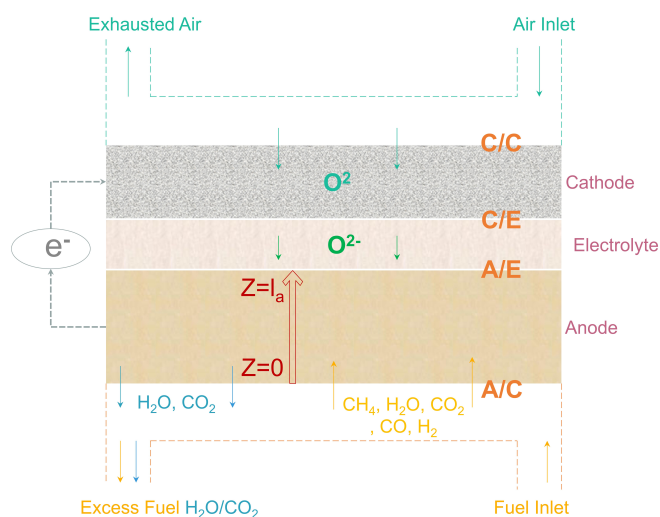
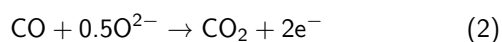
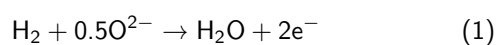


Figure 1. Schematic diagram of SOFC with oxide ion conducting electrolyte.

The following electrochemical reactions are considered in the study:



In Equations (1) and (2), 2 moles of ionic charge transfer occur for every mole of H₂ or CO ionized. Thus, the total moving charge Q is 2F. At the same time, 2 moles of elec-

tronic charge transfer occur for every mole of H₂O or CO₂ produced. Thus, the total moving charge Q is -2F. The Faraday's constant F represents the electric charge per mole of electrons. As per the literature, the characteristic reaction times of reactions in Equations (1) and (2) are 10⁻⁷ and 10⁻⁵ second respectively (Milewski and Lewandowski, 2011). Again, the rate constants for reactions in Equations (1) and (2) are 2.5 × 10¹⁸ (m, mol, s) and 1.9 × 10¹³ (m, mol, s) respectively (Zhu et al., 2005). The reactions are very fast. Whereas, the diffusion time constant for fuel components is close to 1 second (Milewski and Lewandowski, 2011). Moreover, at 1023.15 K, the reactant diffusivity of 1.5 cm²/s and 0.4 cm²/s are reported in the literature for H₂ and CO respectively (Modjtahedi et al., 2016). Clearly, the slower rate of diffusion may hinder the process. Thus, the limit posed by molecular and Knudsen diffusion are extensively analyzed in this study. Surface diffusion is not considered in the study. Interested readers may refer to another source (Vogler et al., 2009).

The simplified 1D system illustrated in Figure 1 is taken from the work of Yakabe et al. (2000) on a porous anode 3D system. The modeling assumptions are consistent with the works of Suwanwarangkul et al. (2003) and Yakabe et al. (2000) for a planar SOFC. The pressure gradient is considered for some models. The modeling assumptions are postulated as follows:

- The gaseous fuel mixtures, H₂-H₂O-Ar and CO-CO₂ are expected to behave ideally. This is a reasonable assumption at high temperature, low pressure and low current density conditions (Vural et al., 2010). The molar concentration at the A/C interface is equal to the bulk concentration ($x_{i,A/C} = x_{i,bulk}$).
- The temperature isotherm and steady state are assumed to be established throughout the anode. The thermal diffusion, surface diffusion and adsorption are ignored to reduce the complexity of modelling. The anode gas diffusion layer is considered to be isotropic. Any change in total pressure in the anode channel is ignored. The diffusion transport remains dominant along the z-direction.
- The depth of the electrochemical reaction zone is very small as compared to anode thickness. Hence, the electrochemical reaction is assumed to take place only at the A/E interface (Lehnert et al., 2000). All the fuel reaching A/E interface is consumed in the electrochemical reaction. As a result, the entire molar mass transport flux reaching A/E interface is converted to the charge flux. The modelling is focused on mass transport only to study factors contributing to diffusion overpotential. The effects of ionic mass transport from the electrolyte end are ignored.
- Uniform gas concentration is assumed along the channel by keeping the length of the anode channel small (20 mm) and limiting the fuel utilization to less than 5%. Consequently, uniform current density can be achieved over the entire anode length.

The diffusion mass transfer equations are solved in the z -direction to calculate the fuel component mole fractions at the A/E interface. For a single component i with mole fraction x_i and molar mass transport flux N_i diffusing through a porous medium with porosity ε , the general form of the equation for mass transfer is given by (Suwanwarangkul et al., 2003):

$$\frac{\varepsilon}{RT} \frac{\partial(x_i P)}{\partial t} = -\nabla \cdot N_i + r_i \quad (3)$$

The term r_i represents the rate of reaction occurring inside the medium for component i . The total pressure across anode denoted by P is measured at A/C interface. The R and T represent the universal gas constant and cell operating temperature respectively. No chemical reactions are occurring inside the medium for the fuel systems considered here. When the electrochemical reactions occur only at the A/E interface and the system is at steady state Equation (3) can be simplified as:

$$\nabla \cdot N_i = 0 \quad (4)$$

Therefore, the molar mass transport flux remains constant over the domain. At the A/E interface, it can be determined using reaction stoichiometry for uniform current density j and Faraday constant F . It is already assumed that the entire molar mass transport flux reaching A/E interface is converted to the charge flux. Thus, the current density is determined by multiplying the total moving charge and molar mass transport flux for each species (O'Hayre et al., 2016). For H_2 it can be written as $j = 2FN_{H_2}$. Thus,

- For the H_2 - H_2O -Ar system:

$$N_{H_2} = \frac{j}{2F} \quad (5)$$

$$N_{H_2O} = -\frac{j}{2F} \quad (6)$$

- For the CO - CO_2 system:

$$N_{CO} = \frac{j}{2F} \quad (7)$$

$$N_{CO_2} = -\frac{j}{2F} \quad (8)$$

2.1. Model parameters

2.1.1. Binary diffusion coefficient

The effective binary diffusion coefficient between gaseous species i and j denoted by D_{ij}^{eff} is calculated using the Fuller et al. correlation (Taylor and Krishna, 1993):

$$D_{ij}^{\text{eff}} = \frac{\varepsilon}{\tau^2} \frac{1.013 \times 10^{-2} T^{1.75} \sqrt{\frac{1}{M_i} + \frac{1}{M_j}}}{P (\sqrt[3]{V_i} + \sqrt[3]{V_j})^2} \quad [\text{m}^2/\text{s}] \quad (9)$$

where V_i represents the specific Fuller diffusion volume for component i . It can be found in Table 2 for the gaseous

fuel components (Taylor and Krishna, 1993). M_i is molecular weight in g/mol. ε and τ^2 stands for porosity and tortuosity factors, respectively.

2.1.2. Knudsen diffusion coefficient

The effective Knudsen diffusion coefficient for component i denoted by D_{iM}^{eff} for a porous medium with pore radius r_p is given by (Poling et al., 2000):

$$D_{iM}^{\text{eff}} = \frac{\varepsilon}{\tau^2} \frac{2r_p}{3} \sqrt{\frac{8RT}{\pi M_i}} = \frac{\varepsilon}{\tau^2} 97r_p \sqrt{\frac{T}{M_i}} \quad [\text{m}^2/\text{s}] \quad (10)$$

In Equation (10), molecular weight M_i is in kg/mol.

2.1.3. Anode permeability

The convective velocity v due to the pressure gradient across anode dP/dz is governed by Darcy's law $v = -\frac{B_0}{\mu} \frac{dP}{dz}$. The permeability of the porous anode denoted by B_0 is calculated by the Kozeny–Carman relationship (Ni et al., 2008). The variation of permeability with pore radius r_p can help further analyze the models.

$$B_0 = \frac{r_p^2 \varepsilon^3}{18\tau^2(1-\varepsilon)^2} \quad [\text{m}^2] \quad (11)$$

2.1.4. Dynamic viscosity

The equation for calculating pure component viscosity can be determined using the Chapman–Enskog theory. The mixture viscosity μ is calculated using Wilke's formula (Poling et al., 2000).

$$\mu_i = \frac{2.669 \times 10^{-7} (M_i T)^{0.5}}{\sigma^2 \Omega_v} \quad [\text{Pa} \cdot \text{s}] \quad (12)$$

$$\mu = \sum_{i=1}^n \frac{x_i \mu_i}{\sum_{j=1}^n x_j \phi_{ij}} \quad [\text{Pa} \cdot \text{s}] \quad (13)$$

$$\phi_{ij} = \frac{1}{\sqrt{8}} \left[1 + \left(\frac{M_i}{M_j} \right) \right]^{-\frac{1}{2}} \left[1 + \left(\frac{\mu_i}{\mu_j} \right)^{\frac{1}{2}} \left(\frac{M_i}{M_j} \right)^{\frac{1}{4}} \right]^2 \quad (14)$$

In Equation (13), the mixture viscosity accounts for an instantaneous change in the mole fraction of a mixture component throughout the system. The collision integral Ω_v is determined by following an empirical equation (Neufeld et al., 1972; Poling et al., 2000). The collision diameter σ for required elements can be found in Table 2 (Poling et al., 2000).

$$\Omega_v = \frac{1.16145}{(k_b T / \omega)^{0.14874}} + \frac{0.52487}{\exp(0.77320 k_b T / \omega)} + \frac{2.16178}{\exp(2.43787 k_b T / \omega)} \quad (15)$$

The experimental parameters were given in Table 1 as taken from the work of Yakabe et al. (2000). The actual path followed by the particle is usually higher than the length of the medium due to the tortuous nature of the porous medium. The tortuosity factor used as a fitting parameter accounts for this occurrence. It is to be noted that the tortuosity factor also accounts for the uncertainties related to diffusion mass transfer models (Vural et al., 2010). The diffusion coefficients, dynamic viscosity and permeability were estimated as discussed in Section 2.1. The diffusion overpotential η_{diff} is the performance parameter for the models discussed. It is defined as loss of cell voltage due to resistance to diffusion mass transfer. The component mole fractions at the A/E interface were calculated using the diffusion mass transfer models. Thereafter, the diffusion overpotential was calculated for the ternary and binary mixtures as follows (Bao et al., 2016).

For H₂/H₂O/Ar system:

$$\eta_{diff} = \frac{RT}{2F} \ln \left(\frac{x_{H_2,bulk} x_{H_2O,A/E}}{x_{H_2,A/E} x_{H_2O,bulk}} \right) \quad (16)$$

For CO/CO₂ system:

$$\eta_{diff} = \frac{RT}{2F} \ln \left(\frac{x_{CO,bulk} x_{CO_2,A/E}}{x_{CO,A/E} x_{CO_2,bulk}} \right) \quad (17)$$

In Equations (16) and (17) the term x_i represents the mole fraction of component i . The bulk mole fractions are

Table 1. Parameters used for model validation.

Parameter	Symbol	Value	Unit
Anode thickness	l_a	2×10^{-3}	m
Operating temperature	T	1023	K
Operating pressure	P	101325	Pa
Universal gas constant	R	8.314	J mol ⁻¹ K ⁻¹
Porosity	ϵ	0.45	
Tortuosity	τ	2.1, 1.9	
Average pore radius	r	1.3×10^{-6}	m

Table 2. Parameters used for calculating mixture viscosity.

Element	σ [Å]	ω/k_b [K]	Specific Fuller Volume V
Hydrogen H ₂	2.827	59.7	6.12
Carbon monoxide CO	3.69	91.7	18
Water H ₂ O	2.641	809.1	13.1
Carbon dioxide CO ₂	3.941	195.2	26.7
Argon Ar	3.542	93.3	16.2

equated to the component mole fractions at A/C interface as a boundary condition at A/C interface. The diffusion overpotential at an H₂ mole fraction of 0.8 and CO mole fraction of 0.64 are taken as reference for specified current densities as described in work by Yakabe et al. (2000). The reference diffusion overpotential is denoted by $\eta_{diff,ref}$. The difference in diffusion overpotential from reference for a range of H₂ and CO mole fractions can be determined as $\Delta\eta_{diff} = \eta_{diff} - \eta_{diff,ref}$.

2.2. Diffusion mass transfer models

For a system with n number of components, the sum of mole fractions is 1 ($\sum_{i=1}^n x_i = 1$). Moreover, the sum of their 1st order differentials is 0, i.e. $\sum_{i=1}^n \frac{dx_i}{dz} = 0$. Such a system of equations offers a set of $n - 1$ independent equations. The molar concentration of fuel components at the A/C interface ($x_{i,A/C}$) and molar mass transport flux (N_i) given by Equations (5)–(8) are taken as boundary conditions.

2.2.1. eSMM

For n -component with total pressure P , the Stefan–Maxwell relation in 1D is given by (Bao et al., 2016),

$$-\frac{P}{RT} \frac{dx_i}{dz} = \left[\sum_{j=1, j \neq i}^n \frac{x_j N_j - x_i N_j}{D_{ij}^{eff}} \right] \quad (18)$$

where N_i is molar mass transport flux for component i (mol m⁻²s⁻¹), D_{ij}^{eff} is binary diffusion coefficient and R is the universal gas constant. Rearranging we get,

$$\frac{dx_i}{dz} = -\frac{RT}{P} \left[\sum_{j=1, j \neq i}^n \frac{x_j N_j - x_i N_j}{D_{ij}^{eff}} \right] \quad (19)$$

For the extended Stefan–Maxwell model, the Knudsen diffusion is taken into account by modifying the binary diffusion coefficient as (Bao et al., 2016),

$$D_{ij,e-SMM}^{eff} = 0.5 \left[\frac{1}{\frac{1}{D_{ij}^{eff}} + \frac{1}{D_{iM}^{eff}}} + \frac{1}{\frac{1}{D_{ji}^{eff}} + \frac{1}{D_{jM}^{eff}}} \right] \quad (20)$$

2.2.2. DGM, DGMFM

The dusty gas model considers total molar flux to be the sum of diffusion flux and viscous flux. The Knudsen diffusion is also taken into account. The model takes an array of pseudo motionless dust particles as one component. After writing the governing equations, the terms relating to the dust particles are removed. The viscous flux term is governed by Darcy's

law. The general form of the dusty gas model in 1D considering molecular diffusion, Knudsen diffusion and viscous drag is given by (Suwanwarangkul et al., 2003):

$$\sum_{i=1, j \neq i}^n \frac{x_j N_i - x_i N_j}{D_{ij}^{\text{eff}}} + \frac{N_i}{D_{iM}^{\text{eff}}} = -\frac{1}{RT} \left[P \frac{dx_i}{dz} + x_i \frac{dP}{dz} \left(1 + \frac{B_0 P}{\mu D_{iM}^{\text{eff}}} \right) \right] \quad (21)$$

The method used by Zhu and Kee (2003) is applied here to find an equation for the pressure gradient. By summing Equation (21) over n -components, the first term on left hand side vanishes. The mole fraction differential term on right hand side sums up to 0 $\left(\sum_{i=1}^n \frac{dx_i}{dz} = 0 \right)$. Therefore, we get:

$$\frac{dP}{dz} = -\frac{\sum_{j=1}^n \frac{N_j}{D_{iM}^{\text{eff}}}}{\frac{1}{RT} + B_0 P \sum_{j=1}^n \frac{x_j}{RT \mu D_{iM}^{\text{eff}}}} \quad (22)$$

By inserting Equation (22) into Equation (21) and rearranging we get:

$$\frac{dx_i}{dz} = -\frac{RT}{P} \left[\sum_{i=1, j \neq i}^n \frac{x_j N_i - x_i N_j}{D_{ij}^{\text{eff}}} + \frac{N_i}{D_{iM}^{\text{eff}}} - x_i \frac{\left(\mu + \frac{B_0 P}{D_{iM}^{\text{eff}}} \right) \sum_{j=1}^n \frac{N_j}{D_{iM}^{\text{eff}}}}{\mu + B_0 P \sum_{j=1}^n \frac{x_j}{D_{iM}^{\text{eff}}}} \right] \quad (23)$$

The dusty gas model was modified in form of Fick's model to construct an explicit analytical expression for molar mass transport flux (Kong et al., 2012). The DGMFM in 1D can be written as (Kong et al., 2014)

$$N_i = -D_i \frac{dc_i}{dz} - c_i \frac{k_i}{\mu} \frac{dP}{dz} \quad (24)$$

The contribution of a third term on the right hand side denoted by symbol N_i^δ was assumed negligible. The molar mass transport flux with the third term can be written as (Kong et al., 2014)

$$N_i = -D_i \frac{dc_i}{dz} - c_i \frac{k_i}{\mu} \frac{dP}{dz} + N_i^\delta \quad (25)$$

where

$$N_i^\delta = \frac{D_i x_i}{1 - x_i} \left[\sum_{j \neq i} \frac{x_j}{D_{ij}^{\text{eff}}} \right] \cdot \left[\sum_{j \neq i} N_j \frac{(1 - x_i)}{D_{ij}^{\text{eff}} D_{iM}^{\text{eff}}} \left(\frac{D_{iM}^{\text{eff}}}{\sum_{j \neq i} \frac{x_j}{D_{ij}^{\text{eff}}}} - \frac{D_{ij}^{\text{eff}}}{\sum_{j \neq i} \frac{x_j}{D_{iM}^{\text{eff}}}} \right) \right] \quad (26)$$

The term $\frac{(1 - x_i)}{D_{ij}^{\text{eff}} D_{iM}^{\text{eff}}} \left(\frac{D_{iM}^{\text{eff}}}{\sum_{j \neq i} \frac{x_j}{D_{ij}^{\text{eff}}}} - \frac{D_{ij}^{\text{eff}}}{\sum_{j \neq i} \frac{x_j}{D_{iM}^{\text{eff}}}} \right)$ indicated as the cancellation factor was expected to be very small. As a result, the contribution of N_i^δ to the total flux becomes small too. In Equation (24), the first and second terms on right hand side account for the diffusive flux and convective flux respectively. Where c_i the molar concentration of component, D_i is the equivalent diffusion coefficient and k_i is the equivalent permeability coefficient. The equations for D_i and k_i can be written as

$$D_i = \frac{1 - x_i}{\sum_{j \neq i} \frac{x_j}{D_{ij}^{\text{eff}}}} D_{iM}^{\text{eff}} \cdot \left(\frac{1 - x_i}{\sum_{j \neq i} D_{ij}^{\text{eff}}} + x_i \frac{1 - x_i}{\sum_{j \neq i} \frac{x_j}{D_{iM}^{\text{eff}}}} + (1 - x_i) D_{iM}^{\text{eff}} \right)^{-1} \quad (27)$$

$$k_i = \frac{B_0 \mu}{P} \frac{1 - x_i}{\sum_{j \neq i} \frac{x_j}{D_{jM}^{\text{eff}}}} D_{jM}^{\text{eff}} \cdot \left(\frac{1 - x_i}{\sum_{j \neq i} D_{ij}^{\text{eff}}} + x_i \frac{1 - x_i}{\sum_{j \neq i} \frac{x_j}{D_{iM}^{\text{eff}}}} + (1 - x_i) D_{iM}^{\text{eff}} \right)^{-1} \quad (28)$$

with $c_i = \frac{P x_i}{RT}$ Equation (24) can be differentiated and rearranged to obtain

$$\frac{dx_i}{dz} = -\frac{RT}{P} \frac{N_i}{D_i} - \frac{dP}{dz} \left[\frac{x_i}{P} + \frac{x_i k_i}{\mu D_i} \right] \quad (29)$$

Similar to DGM, Equation (29) can be summed over n -component with $\sum_{i=1}^n x_i = 1$ and $\sum_{i=1}^n \frac{dx_i}{dz} = 0$ to obtain an equation for the pressure gradient.

$$\frac{dP}{dz} = -\frac{RT \sum_{i=1}^n \frac{N_i}{D_i}}{1 + \frac{P}{\mu} \sum_{i=1}^n \frac{x_i k_i}{D_i}} \quad (30)$$

By inserting Equation (30) into Equation (29) and rearranging we get:

$$\frac{dx_i}{dz} = -\frac{RT}{P} \frac{N_i}{D_i} + \left[\frac{x_i}{P} + \frac{x_i k_i}{\mu D_i} \right] \frac{RT \sum_{i=1}^n \frac{N_i}{D_i}}{1 + \frac{P}{\mu} \sum_{i=1}^n \frac{x_i k_i}{D_i}} \quad (31)$$

2.2.3. BFM, MBFM

The general equation of binary friction model for the n -component system in 1D can be written as (Kerkhof, 1996; Vural et al., 2010):

$$\frac{dx_i}{dz} = \frac{\tau^2 RT}{\varepsilon P} \cdot \left[\sum_{i=1, j \neq i}^n \psi_{ij} \frac{x_i N_j - x_j N_i}{D_{ij}} - N_i f_{im} \right] - \frac{x_i}{P} \frac{dP}{dz} \quad (32)$$

where ψ_{ij} is the diffusion averaging factor for gases. Following the recommendation in Kerkhof's work (Kerkhof, 1996; Vural et al., 2010), its value is set to 1 in this work. D_{ij} is binary diffusion coefficient. The wall-friction coefficient f_{im} is given by:

$$f_{im}^{BFM} = \left(0.89 D_{iM} + \frac{B_0}{\kappa_i} \right)^{-1} \quad [m^{-2}s] \quad (33)$$

The term κ_i is fractional viscosity coefficient.

$$\kappa_i = \frac{\mu_i}{P \sum x_j \phi_{ij}} \quad [s] \quad (34)$$

The equation for pressure gradient can be obtained by summing Equation (32) over n -components.

$$\frac{dP}{dz} = -\frac{\tau^2 RT}{\varepsilon} \sum_{i=1}^n N_i f_{im} \quad (35)$$

By inserting Equation (35) into Equation (32) and rearranging we get:

$$\frac{dx_i}{dz} = \frac{\tau^2 RT}{\varepsilon P} \cdot \left[\sum_{i=1, j \neq i}^n \psi_{ij} \frac{x_i N_j - x_j N_i}{D_{ij}} - N_i f_{im} + x_i \sum_{i=1}^n N_i f_{im} \right] \quad (36)$$

While calculating the diffusion coefficient for the binary friction model the ratio ε/τ^2 was not included in the equation. The work of Pant et al. (2013) modifies the binary friction model by replacing the fractional viscosity coefficient with χ_i . This modification enables the model to take diffusion slip effect into account for components with very different molecular masses.

$$\chi_i = \frac{\mu M_i^{0.5}}{P \sum_{j=1}^n x_j M_j^{0.5}} \quad (37)$$

The fractional viscosity coefficient for the modified binary friction model is given by:

$$f_{im}^{MBFM} = \left(0.89 D_{i,K} + \frac{B_0}{\chi_i} \right)^{-1} \quad [m^{-2}s] \quad (38)$$

2.2.4. MFM

Generally, the standard FM is considered unsuitable for multicomponent mass transfer. The MFM replaces the diffusion coefficient with the effective Fickian diffusion coefficient and partially considers the cross terms in the flux-driving force matrix (Bao et al., 2016; Krishna and Wesselingh, 1997). The equation for the modified Fickian model is obtained by considering viscous flow velocity and neglecting the molar average flow velocity (Bao et al., 2016). The mole fraction differential of species i for an n -component system in 1D is given by:

$$\frac{dx_i}{dz} = -\frac{RT}{P D_i^{\text{eff}}} \left[N_i - x_i \sum_{i=1}^n N_i \right] \quad (39)$$

where D_i^{eff} stands for effective Fickian diffusion coefficient. By neglecting the pressure gradient term in DGM (Bao et al., 2016), the effective Fickian diffusion coefficient can be determined as

$$\frac{1}{D_i^{\text{eff}}} = \sum_{i=1, j \neq i}^n \frac{x_j - x_i (N_j/N_i)}{D_{ij}^{\text{eff}}} + \frac{1}{D_{iM}^{\text{eff}}} \quad (40)$$

All the diffusion models discussed below were solved in MATLAB 15 using ode45 algorithm. The algorithm is based on Runge-Kutta (4th-order 5th-order) formula with variable step size. The relative and absolute tolerances were set to 10^{-3} (0.1%) and 10^{-6} (0.0001%) respectively. In order to numerically solve the models' equations with a 2.5 GHz processor powered computer the time required in seconds are listed as follows. It took 0.788 s, 0.823 s, 0.950 s, 1.760 s, 0.858 s, 1.106 s (ternary system) and 0.620 s, 0.595 s, 0.695 s, 0.876 s, 0.642 s, 0.743 s (binary system) for MFM, eSMM, DGM, DGMFM, BFM and MBFM respectively.

3. RESULT DISCUSSION

3.1. Model validation

The input parameters used to validate the models are taken from experimental work by Yakabe et al. (2000). They are listed in Table 1. The open circuit voltage of SOFC for the ternary fuel system was unrestrained from fuel composition by fixing the ratio of H₂ mole fraction to H₂O mole fraction at 4:1. The H₂ concentration was varied by diluting the fuel mixture using an inert species Ar. The tortuosity factor was used as a fitting parameter. Its values were set to 4.41 and 3.61 for ternary and binary systems respectively. It should be noted that the tortuosity factor was taken as the square of tortuosity in all models. The use of same tortuosity factor for all the models should help identify the differences between the models. The MFM and eSMM models did not include the effect pressure difference across anode. As shown in Figures 2(a-c) and 3(a-c), the differences in diffusion overpotential from the reference for models and experimental data

are plotted against the range of H₂ mole fraction and CO mole fraction for ternary and binary systems, respectively. As reported in previous works, the diffusion overpotential increases with an increase in current density or decrease in fuel concentration (Suwanwarangkul et al., 2003). The new models included in this study such as DGMFM and MBFM also follow a similar trend. At lower current densities and higher fuel concentrations, the change in the diffusion overpotential follows a linear curve. As a principle, for a specified pore radius value, there exists a higher threshold limit for current density and a lower threshold limit for fuel concentration. Beyond these threshold limits, the change in the diffusion overpotential follows an exponential curve. For the given case, the low fuel concentration value lies between 0.2–0.4 H₂ mole fraction and 0.4–0.5 CO mole fraction at all current densities presented in the study. The threshold limits appear when the rate of diffusion of reactants becomes unable to keep pace with the rate of consumption of reactants to produce high current. These limits can vary with the pore radius value.

The percentage deviations of model results from the experimental data are shown in Figures 2(d–f) and 3(d–f). This is an attempt to quantify the difference in prediction efficacy of the models as compared to the experimental measurements. The values of percentage deviation were taken positive when a model underestimated diffusion overpotential. The values of percentage deviation were taken negative when a model overestimated diffusion overpotential. Thus, a lower absolute value of percentage deviation means the model's prediction is closer to the experimental data. The average percentage deviation (avg. dev.) was calculated for each model at all current densities to evaluate the models' efficacy over a range of fuel composition. Moreover, the average percentage deviation can help determine a model's consistency over a wide range of parameters.

For the ternary system, at medium current density, the models are closest to the experimental results. BFM is the best performing model with avg. dev. of 0.2%. The DGM and MBFM offer good prediction with avg. dev. close to 1%. At low current density, the BFM underestimates the diffusion over potential with avg. dev. above 3%. The MFM and DMG outperform the BMF by avg. dev. of less than 1%. At low and medium current density, the DGM avg. dev. remains below 3%, whereas the DGMFM avg. dev. goes above 8%. Therefore, the difference between the models' prediction is about 5%. At the same time, the difference between the MFM and DGM avg. dev. remains below 0.2% despite the exclusion of the pressure gradient effect in MFM. The high efficiency of MFM may be attributed to the partial consideration of cross terms discussed in Section 2.2.4. For the binary system, the models do not perform as well. The percentage deviation for all the models does not fall below 15%. Therefore, the average percentage deviations do not reflect the actual efficacy of the models. On the other hand, by observing Figures 3(a–c), it can be recognized that the models'

predictions follow a trend similar to the experimental data. The diffusion overpotential value goes above the reference for CO mole fraction below 0.36–0.46 for both experimental data and models' prediction. Moreover, the accuracy of the models' prediction increases after the diffusion overpotential value goes above the reference. At low and medium current density, the percentage deviation of the BFM is about 3% less than the DGM. At low current density, the models match the experimental result for binary system. The MFM, DGM and DGMFM are an exact match with avg. dev. of 6.61%. The DGM and DGMFM overlap at other current densities too. This is because the cancellation factor, a term discussed in Section 2.2.2, becomes zero for the binary system in the DGMFM model. Nevertheless, a further study over a wide range of parameters may produce a different outcome.

The empirical inclusion of the Knudsen diffusion term in eSMM without proper scientific explanation leads to high average percentage deviation above 12% for both fuel systems. For the ternary system at low and medium current density, the eSMM massively overestimates the diff over potential. For the binary system, it greatly underestimates the diffusion overpotential at most fuel compositions considered in the study. The avg. dev. of MBFM is about 1% higher than the DGM at all current densities for both systems. After modification, the MBFM predictions are similar to the BFM in most scenarios. The difference between avg. dev. for both models does not exceed 0.5% for either fuel system. However, this small difference can help identify the effect of diffusion slip under SOFC working conditions. At high current density, the models fail to accurately predict the diffusion overpotential for both fuel systems. The avg. dev. rises above 80% and the models massively underestimate the diffusion overpotential. Such deviations may have been caused by the assumptions such as uniform current density and uniform gas concentration along the channel. Furthermore, low fuel utilization may lose validity at high current density. The effects of surface diffusion may be another contributing factor (Bao et al., 2016). A multi-dimensional model that accounts for the depletion of fuel concentration along the channel may be of some help under such circumstances (Tseronis et al., 2008).

The measurement error for diffusion overpotential under SOFC operating conditions may cause error in evaluating the efficiency of the models (He et al., 2014). For SOFC operating conditions the typical leakage current of 0.01 A/m² and uncertainty in temperature measurement (ΔT) in the range of 2.5–5 °C are reported in the literature (O'Hayre et al., 2016). Moreover, typical gas leak (Δx_i) for high temperature SOFC around 0.1–3% leads to measurement error for diffusion overpotential (Chou et al., 2022). The gas leak phenomenon also accounts for the effect of uncertainty in pressure measurement (He et al., 2014). The models' predictions are similar to experimental data at medium and low current density for ternary and binary system respectively. Therefore, compensating for these factors in Equations (5)–

(40), the percentage deviation for the models were evaluated again. For the ternary system, with leakage current of 0.01 A/m² and ΔT value of 5 °C, the avg. dev for the models changed to MFM (-0.08), eSMM (-14.01), DGM (-0.39), DGMFM (11.11), BFM (-2.20) and MBFM (-2.80). The MFM and DGM were able to better compensate for the error as compared to the other models. In addition, after including Δx_{H_2} value of 3% the avg. dev for the models changed to

MFM (-12.01), eSMM (-25.83), DGM (-12.32), DGMFM (-0.82), BFM (-14.12) and MBFM (-14.73). Either the models lose efficacy or inappropriately compensate for the gas leak. However, the DGMFM is an exception. The reason for increase in accuracy may be attributed to exclusion of the N_i^δ term. For the binary system, the average percentage deviations do not reflect the actual efficacy of the models. Therefore, it is futile to include results on measure-

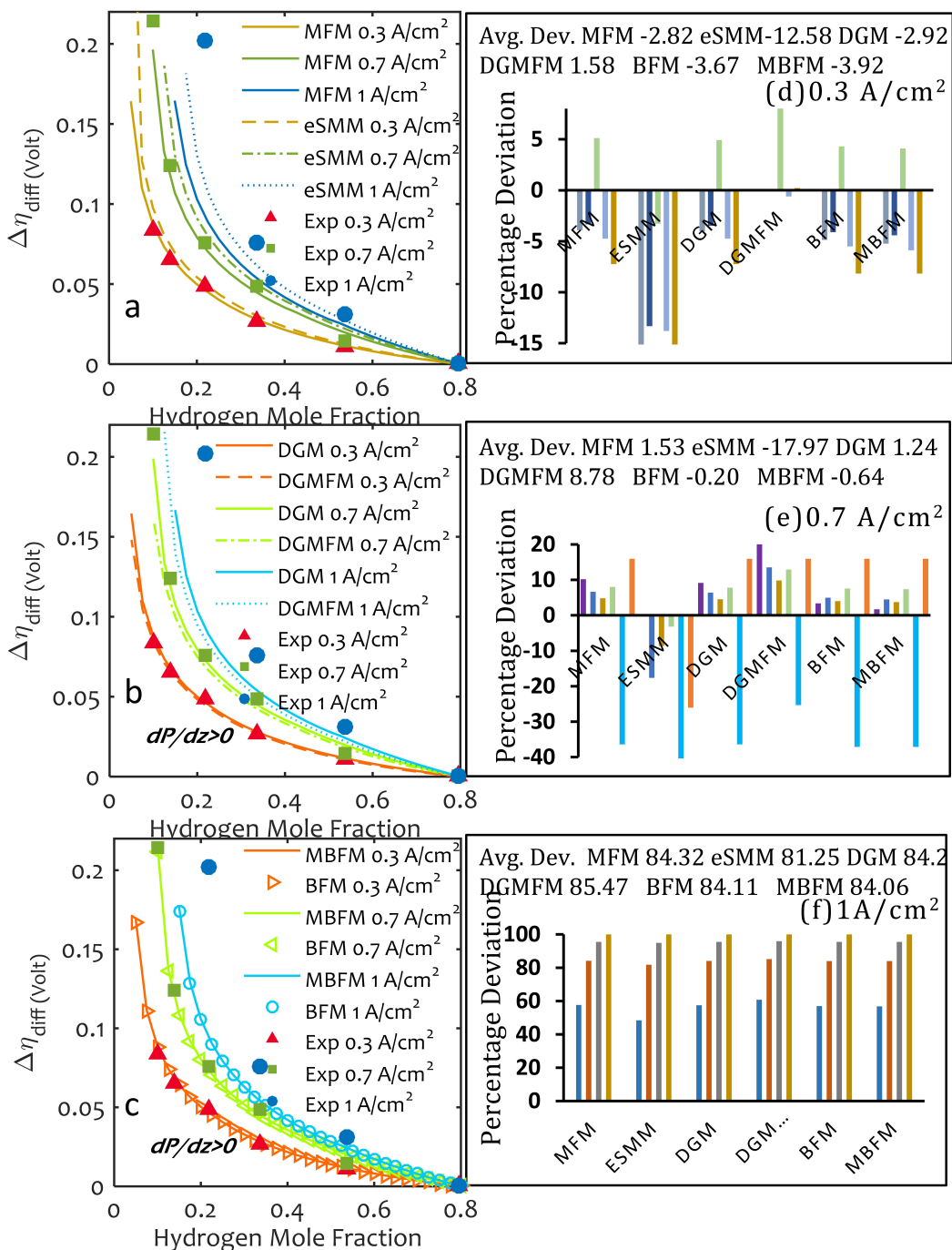


Figure 2. (a–c) Comparison between model prediction and experimental data of difference in diffusion overpotential from the reference ($\Delta\eta$) for the ternary system at different current densities; (d–f) deviation for model prediction from experimentally determined data points. H₂ mole fraction for (d–f) from left to right are (d) 0.10, 0.14, 0.22, 0.34, 0.54 (e) 0.10, 0.14, 0.22, 0.34, 0.54, 0.79 (f) 0.22, 0.34, 0.54, 0.79.

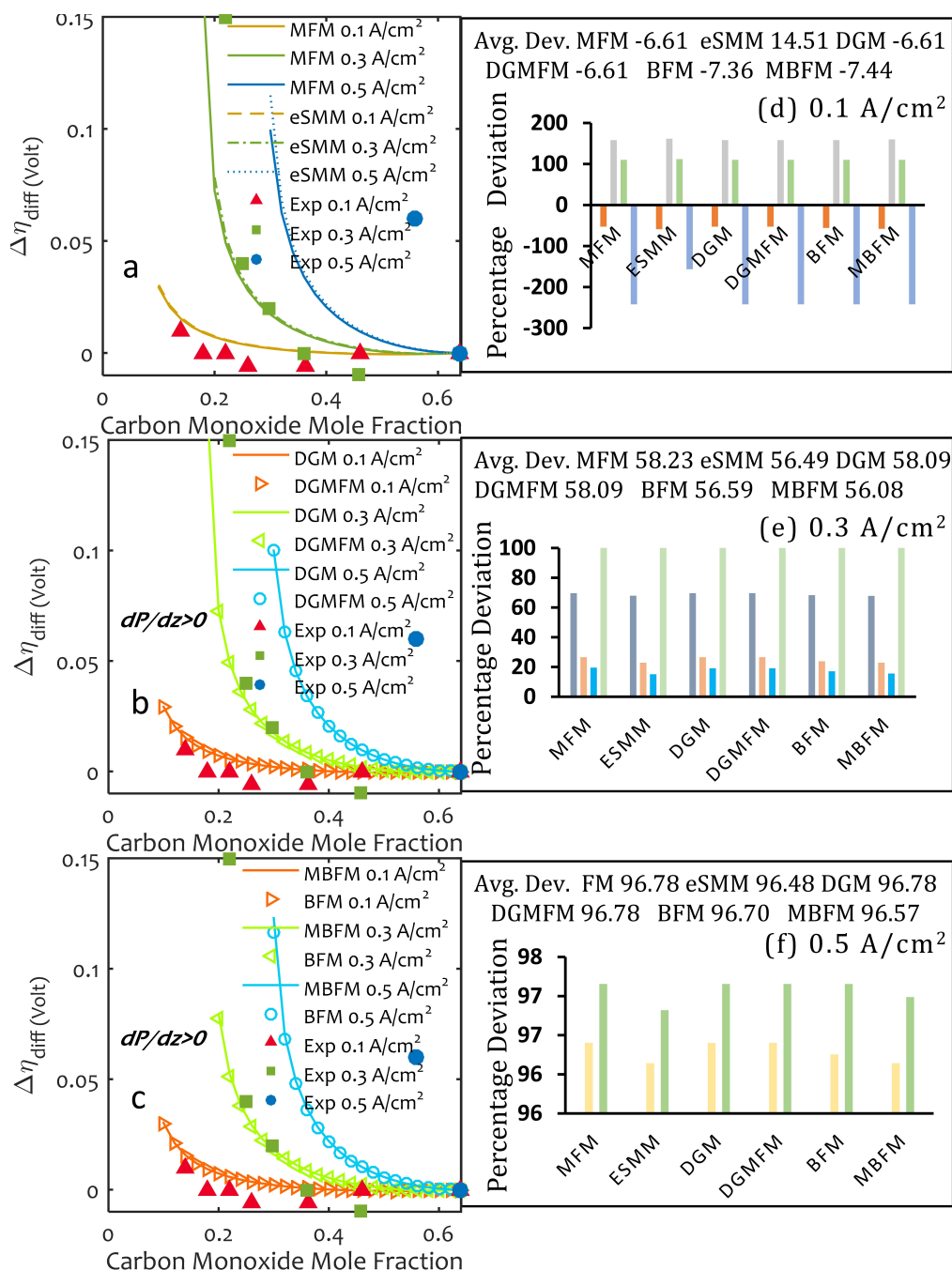


Figure 3. (a–c) Comparison between model prediction and experimental data of difference in diffusion overpotential from the reference ($\Delta\eta$) for the binary system at different current densities; (d–f) deviation for model prediction from experimentally determined data points. CO mole fraction for (d–f) from left to right are (d) 0.13, 0.25, 0.36, 0.46 (e) 0.21, 0.24, 0.30, 0.46 (f) 0.46, 0.56.

ment error for diffusion overpotential. In general, the DGM offers an excellent prediction for the experimental parametric conditions. At the same time, the MFM, MBFM and DGMFM offer good prediction of the diffusion overpotential among the other models tested for a set of pre-fixed parameters. However, these models may respond differently to further changes in parameters. Hence, more analysis of the models' efficacy over a wider range of parameters is necessary.

3.2. Effect of pore radius and current density

A higher pore radius is preferable to minimize the diffusion overpotential. When the pore radius is low enough and the current density is high, the effect of diffusion overpotential is maximum. The difference between the models looks ever so small for the fixed set of parameters used so far. It is probable the models will diverge more when a diverse set of parameters are introduced.

Furthermore, the models need to be evaluated beyond the experimental operating conditions. Therefore, the range of pore radius and current density were adjusted to further assess the models' efficacy. The pore radius was reduced from 1 μm to 0.1 μm . Further reduction of the pore radius may result in an imaginary number value for diffusion overpotential as the diffusion of reactants ceases to take place. The current density range was extended to 0–2 A/cm^2 for the ternary system and 0–0.7 A/cm^2 for the binary system. The fuel component mole fraction was varied between 0.2 to 0.8 and 0.24 to 0.64 for ternary and binary systems respectively.

The increase in current density or decrease in pore radius leads to a shortage of fuel at the A/E interface and an increase in diffusion overpotential. Despite the difference in exact predictions, the models do follow a similar trend for any change in parametric conditions. Hence, a critical analysis of this trend is presented prior to a comparative study of the models. The effect of pore radius over a wide range of current density can be observed in Figures 4 and 6. In Figures 8 and 10 the diffusion overpotential is plotted against a range of pore radius at high, moderate, low fuel concentration and fixed moderate current density. The molecular diffusion dominates for pore radius above 0.6 μm . In Figure 4, for the ternary system, when the pore radius is reduced from 1 μm to 0.6 μm at a current density of 1 A/cm^2 and H_2 mole fraction of 0.65, the change in diffusion overpotential is about 25 mV. Beyond this point, the difference increases rapidly with further increase in current density or decrease in pore radius value. The difference in diffusion overpotential almost doubles for each 0.5 A/cm^2 increase, when the pore radius is reduced from 1 μm to 0.6 μm . Similar results are also observed for the binary system.

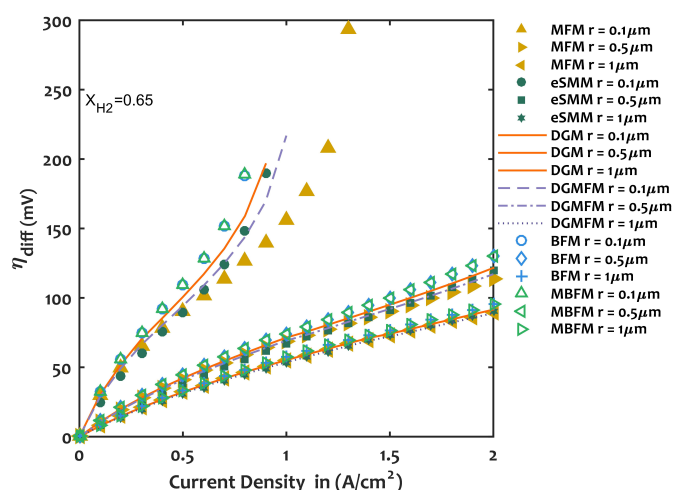


Figure 4. Effect of pore radius on diffusion overpotential for a range of current density at fixed fuel concentration, ternary system.

In Figure 6, for the binary system, when the pore radius is reduced from 1 μm to 0.6 μm at a current density of 0.3 A/cm^2 and CO mole fraction of 0.48, the change in diffusion over-

potential is about 10 mV. The difference in diffusion overpotential almost doubles for each 0.2 A/cm^2 increase. At pore radius value of 0.1 μm , the diffusion overpotential rapidly increases for both fuel systems for a small change in current density. It increases from 100 to 200 mV between 0.6–0.9 A/cm^2 for the ternary system and 40 to 80 mV between 0.1–0.2 A/cm^2 for the binary system. The limiting current density drops below 1 and 0.2 A/cm^2 at a pore radius value of 0.1 μm for the ternary and binary system, respectively. In Figures 8 and 10 for both fuel systems, the rapid change in diffusion overpotential for pore radius below 0.6 μm can be noticed at all fuel concentrations, even though, the current density is fixed to a moderate value.

This happens due to a substantial upsurge in the rate of wall molecule interaction at low pore radius. Therefore, the pore radius should not be reduced below 0.6 μm to avoid any extra increase in diffusion overpotential due to the increased rate of wall molecule interactions. This condition also applies even if it is suitable to reduce pore radius to maximize A/E interface surface area or TPB capacity. The difference between the models' predictions are shown in Figures 5, 7, 9 and 11.

It is quantified in mV of diffusion overpotential difference for the set of parametric conditions applied. The DGM is considered as a reference model due to its widespread use in SOFC studies. The difference between BFM and MBFM prediction is shown in Figures 5f, 7f, 9f, and 11f. The cause of major difference between the models for pore radius below 0.6 μm can be attributed to an increase in the number of wall molecule interactions.

The mixture viscosity, permeability, pressure difference and the Knudsen diffusion are all affected due to change in the rate of wall molecule interactions. In Figures 5 and 9, for the ternary system, the maximum difference between BFM and MBFM remains in the range of 0.2–0.8 mV for the entire range of pore radius, fuel concentration and high current density. The effect of diffusive slip remains small due to the tiny size of H_2 and H_2O molecules. Thus, both models predict similarly. At low and medium current, the MFM can give predictions similar to the DGM as long as the Knudsen diffusion is not dominant. Under these parametric conditions, in Figure 9c, the MFM is closest to the DGM with a maximum difference of around 2 mV. Moreover, the pressure difference effects exclusion in MFM does not affect the predictions severely although the MFM falls behind the DGM exceedingly at high current or small pore radius. The difference between DGM and MBFM prediction remains in the range of 2–5 mV for pore radius above 0.6 μm irrespective of the H_2 concentration at any current density. At low pore radius, the MBFM predictions are 5–15 mV higher than the DGM depending on the H_2 concentration. The difference remains in the range of 2–8 mV for any change in current density. Thus, the MBFM can be a good alternative to the DGM for multi-component systems. The DGMF falls behind DGM as fuel concentration decreases or current density increases.

As the H_2 concentration decreases, the difference can increase up to 35 mV depending on the pore radius. Similar to the MBFM, the difference remains in the range of 2–10 mV for any change in current density. At large pore radius, the DGMFM can easily replace the DGM for multi-component systems.

In Figure 5, the difference between the DGM and eSMM increases up to a certain point followed by sharp decrease. The point of transition varies with pore radius and current density. In Figure 9, at high H_2 concentration, the eSMM predictions are lower than the DGM by 2–20 mV. As the H_2 concentration decreases, the eSMM predictions are higher than the

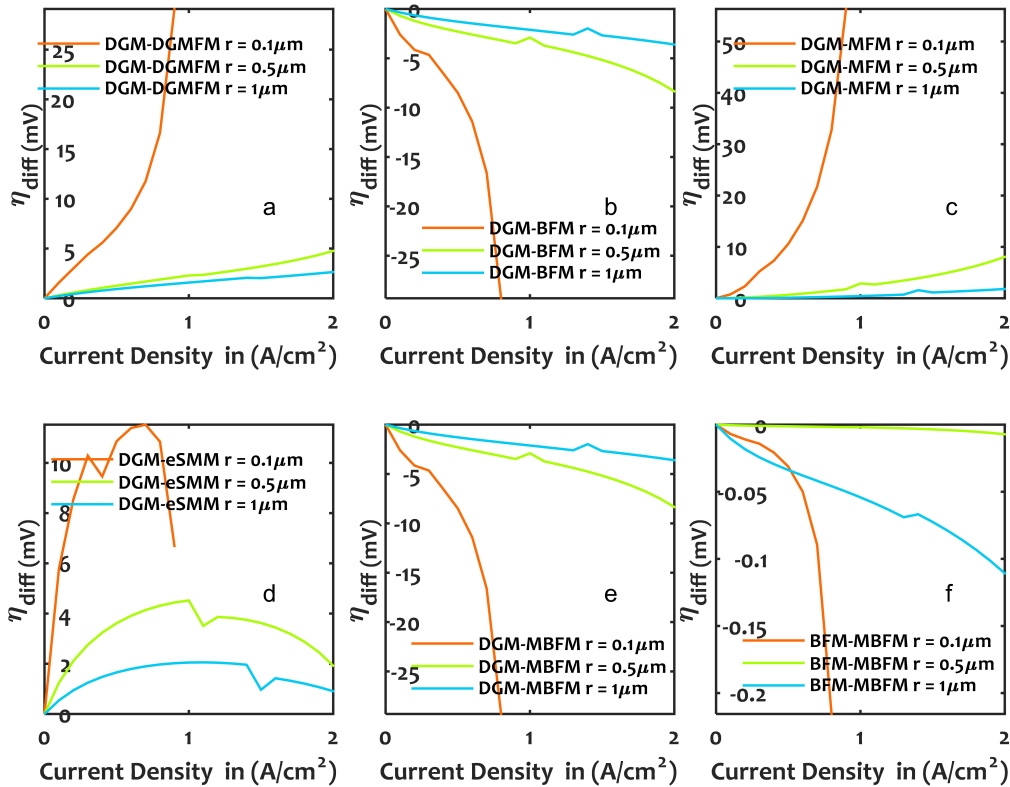


Figure 5. (a–f) difference between the models' prediction for a range of current density at fixed fuel concentration, ternary system.

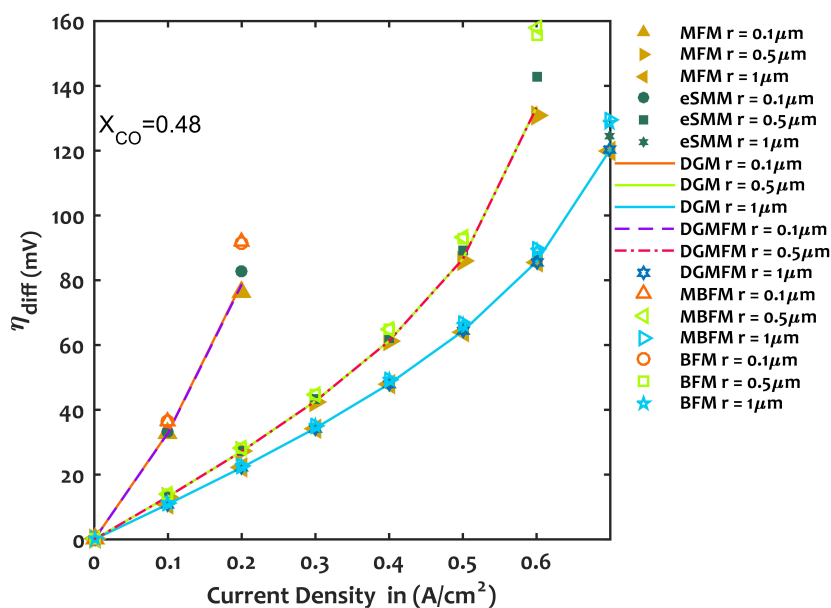


Figure 6. Effect of pore radius on diffusion overpotential for a range of current density at fixed fuel concentration, binary system.

DGM by 1–50 mV. It means that the eSMM underestimates the rate of diffusive flux at high H_2 concentration. As the H_2 concentration decreases, the eSMM tends to overestimate the rate of diffusive flux. Due to such irregularity in prediction, the eSMM may not a viable choice for multi-component systems.

In Figures 7 and 11, for the binary system, the maximum difference between BFM and MBFM exists in the range of 2–5 mV for the entire range of pore radius, fuel concentration and high current density. The effect of diffusive slip is greater than the ternary system due to the large size of CO and CO_2 molecules. Furthermore, the effect of diffusive slip increases

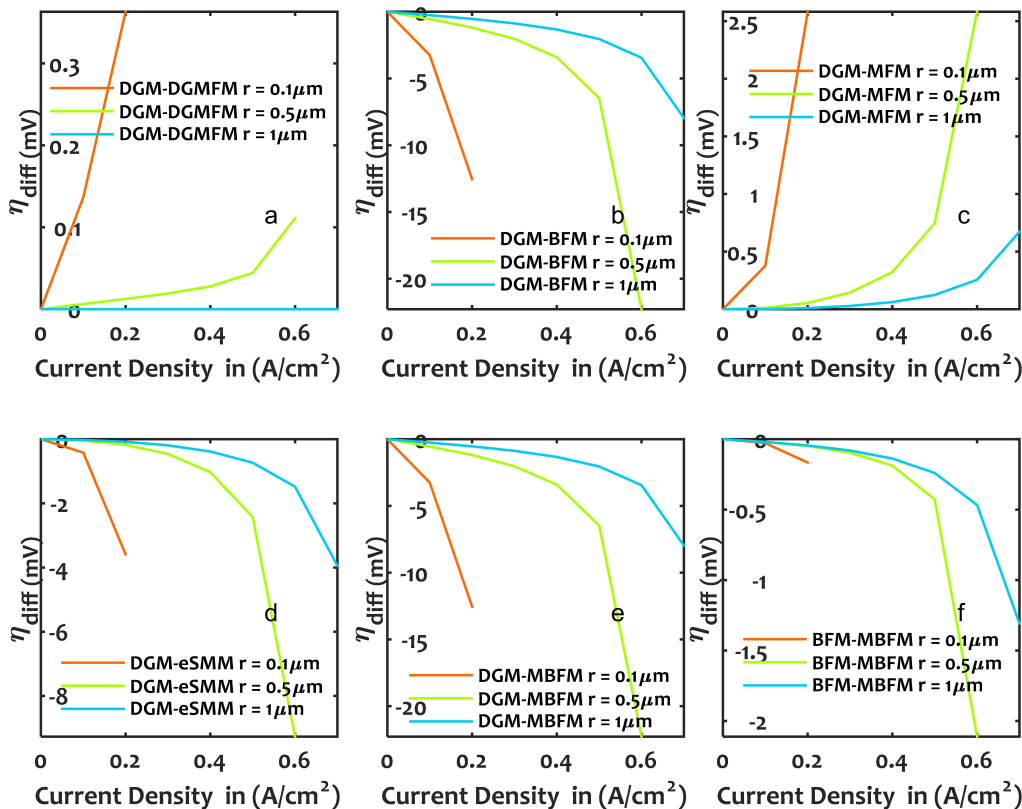


Figure 7. (a–f) difference between the models' prediction for a range of current density at fixed fuel concentration, binary system.

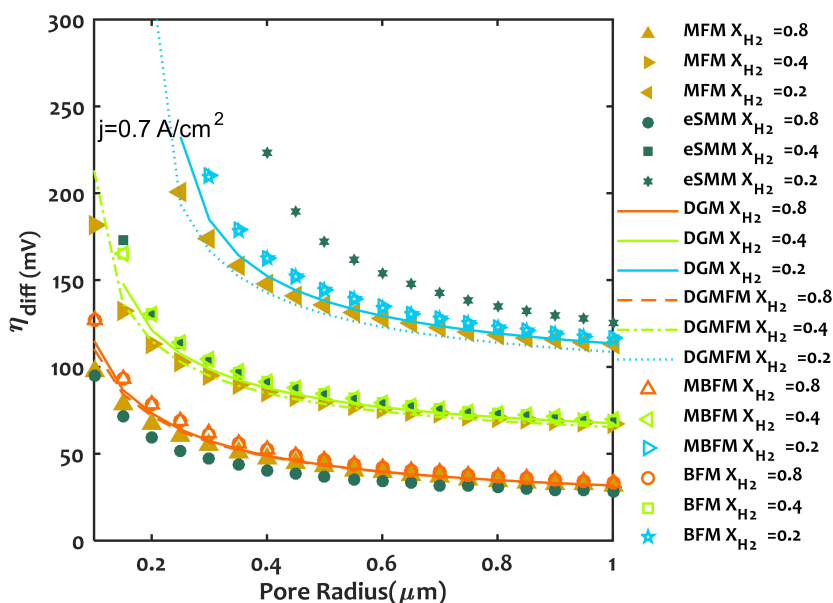


Figure 8. Effect of pore radius on diffusion overpotential at different fuel concentrations for a fixed current density, ternary system.

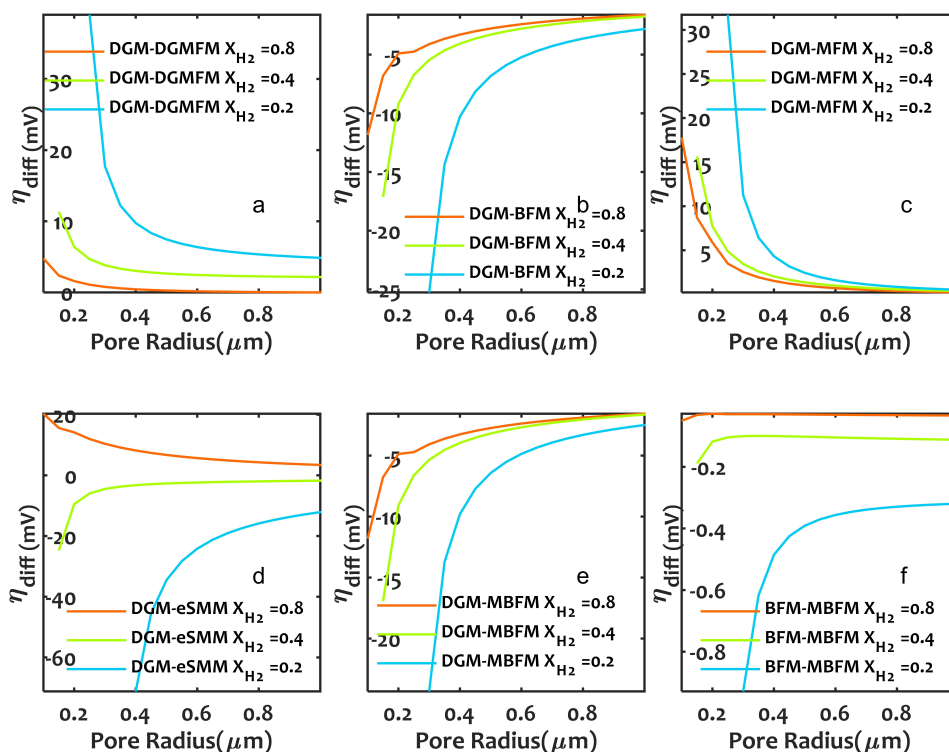


Figure 9. Difference between the models' prediction with change in pore radius at different fuel concentrations for a fixed current density, ternary system.

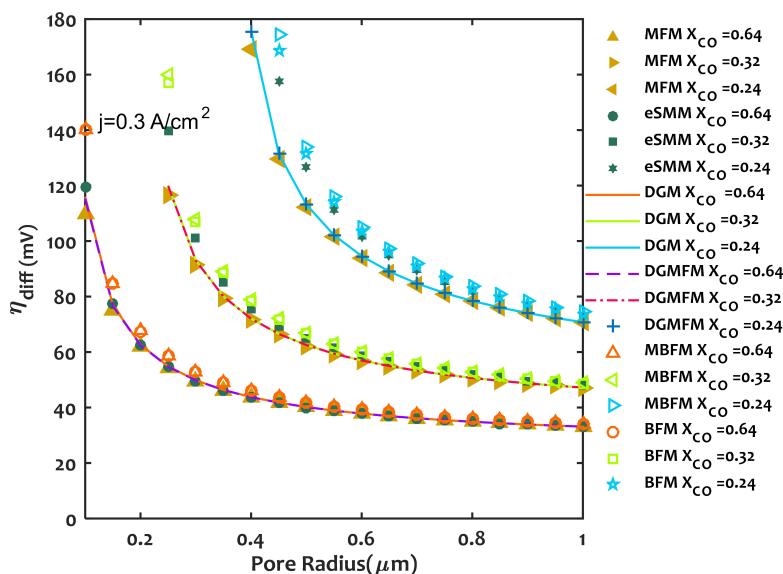


Figure 10. Effect of pore radius on diffusion overpotential at different fuel concentrations for a fixed current density, binary system.

with decrease in pore radius or increase in current density. At high pore radius the difference between MFM and DGM does not exceed 1 mV. At low pore radius the difference can go up to 2 mV. The current density does not have any significant effect either. The maximum difference does not exceed 5 mV. Thus, the MFM can be used for a binary system to lessen computational cost. At large pore radius, the difference between the MBFM and DGM does not exceed 5 mV.

At low pore radius, the difference becomes significant only for high current density and low CO concentration. Under these parametric conditions, the difference can go beyond 15 mV. Hence, the MBFM can be a good alternative to the DGM as long as the pore radius does not drop below $0.6 \mu\text{m}$. At low pore radius, the difference between DGM and eSMM exists in the range of 2–8 mV for the parametric conditions used here. The eSMM overestimates the Knudsen diffusion at low fuel

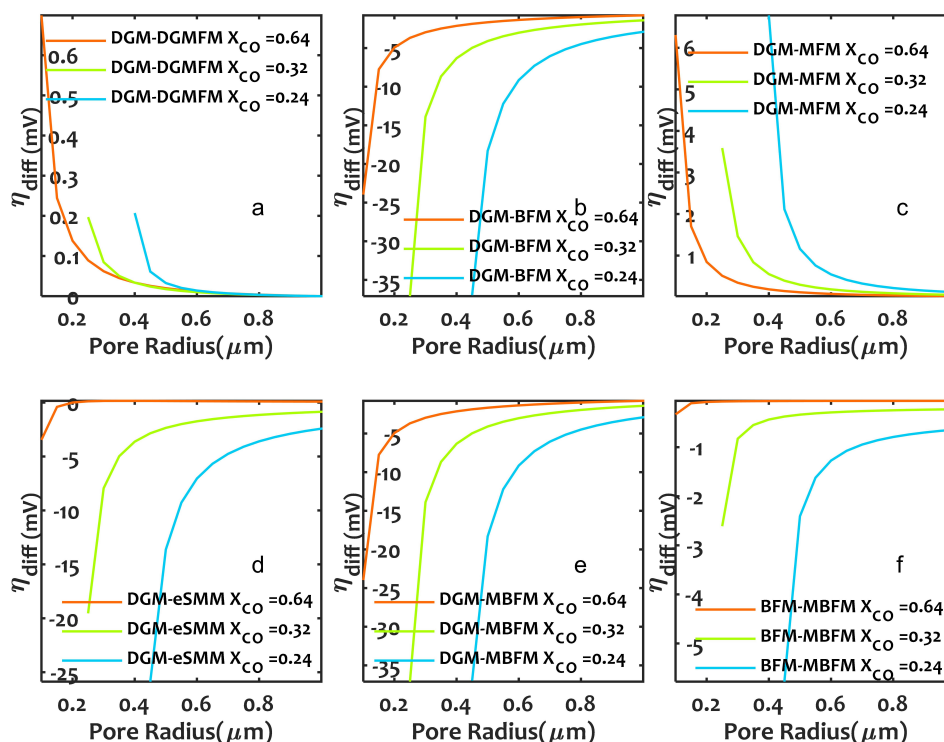


Figure 11. Difference between the models' prediction with change in pore radius at different fuel concentrations for a fixed current density, binary system.

concentration by 5 to 25 mV. Unlike the Kong et al. (2012) hypothesis, the DGMFM is not an exact match of DGM. Even though the cancellation factor in Equation (26) is zero for the binary system, there is still some difference between the DGM and DGMFM. Nevertheless, the maximum difference between the DGMFM and DGM resides in the range of 0.3–0.6 mV. The predictions made by the DGMFM are closest to the DGM for the binary system.

Beyond the experimental conditions, for the broad range of parameters applied, the accuracy of eSMM is questionable under SOFC anode conditions. The MFM, DGMFM and MBFM can predict the diffusion overpotential efficiently depending upon parametric conditions.

3.3. Effect of pressure gradient

The pressure gradient in the SOFC anode can be present due to various reasons. The momentum loss caused by the wall molecule collision for a gaseous system having components of different molecular weights is most common (Wang et al., 2012). The pressure gradient in the SOFC anode can be present if there is a net change in the number of moles in the gaseous phase after the electrochemical reaction (Suwanwarangkul et al., 2003). Moreover, a decrease in permeability leads to an increase in the pressure gradient. However, the anode permeability being a function of pore radius, any study involving a change in pore radius also reflects the effects of change in permeability. Therefore, further study on this aspect is not required.

In both fuel systems applied in this study, there is no net change number of moles in the gaseous phase. Although the molecular weights of the fuel components are very different, the contribution of pressure gradient due to convective transport is small. Ultimately, its contribution to the diffusion overpotential may be negligible for large pore radius and therefore the model validation.

The results obtained from difference in DGM, DGMFM, BFM and MBFM with and without the pressure gradient are plotted in Figure 12. The reference diffusion overpotential was calculated with and without the pressure gradient as per requirement. Under the pre-fixed operating conditions used for the model, validation proves the effect of pressure difference to be minimal. The difference resides around 0.6 mV and 0.1 mV for the majority of H₂ and CO concentration range, respectively, although the results obtained are not free of error when the pressure gradient is ignored for the ternary system. In case of the binary system, all the models tested overlap for the entire range of test parameters used in the experiment. In such a scenario, it is safe to ignore the pressure gradient. The pressure gradient increases as the pore radius is reduced or current density is increased. Therefore, the effect of pressure gradient needs to be assessed further at lower pore radius, high current density and low fuel concentration to determine the criteria for its inclusion in the ternary system. In Figure 13, the parametric conditions applied in Figures 4 and 6 are reapplied for the DGM, DGMFM, BFM and MBFM with and without the pressure gradient.

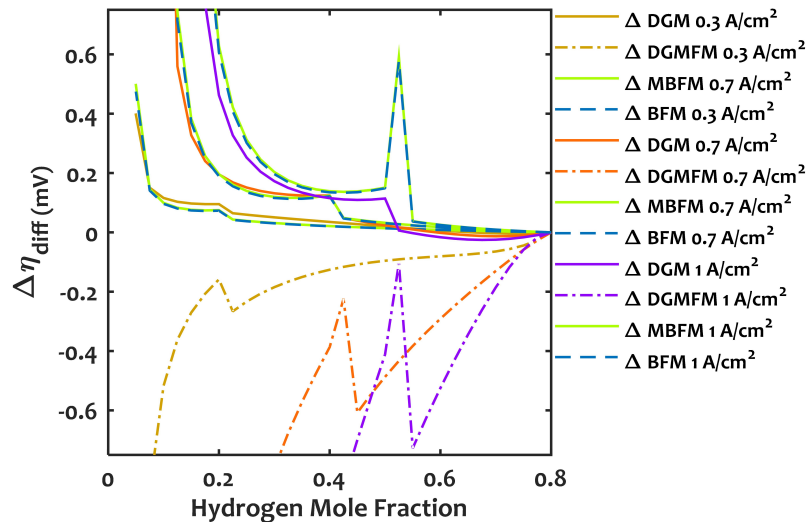


Figure 12. Comparison of the difference in diffusion overpotential from the reference ($\Delta\eta$) predicted by various models with and without the pressure gradient for ternary.

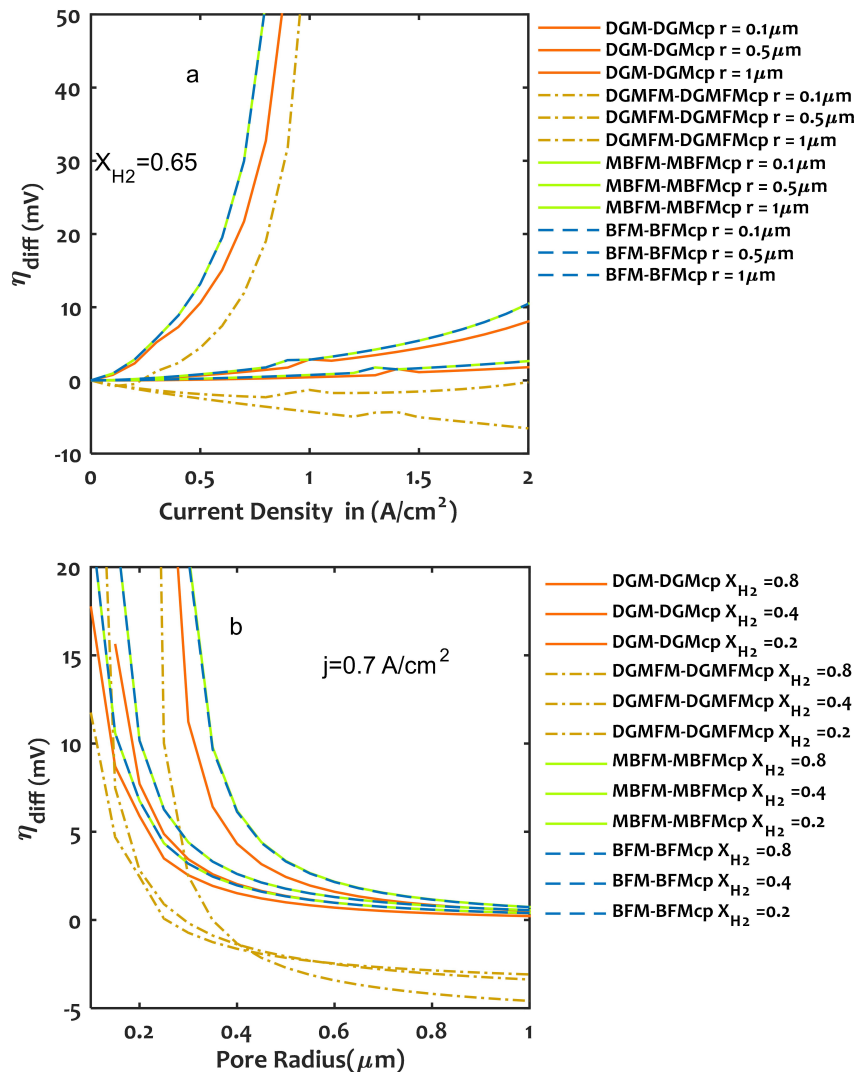


Figure 13. Comparison of pore radius effect predicted by DGM, DGMFM, BFM and MBFM with and without the pressure gradient; (a) for a range of current density, (b) at low, moderate and high fuel concentration for ternary system.

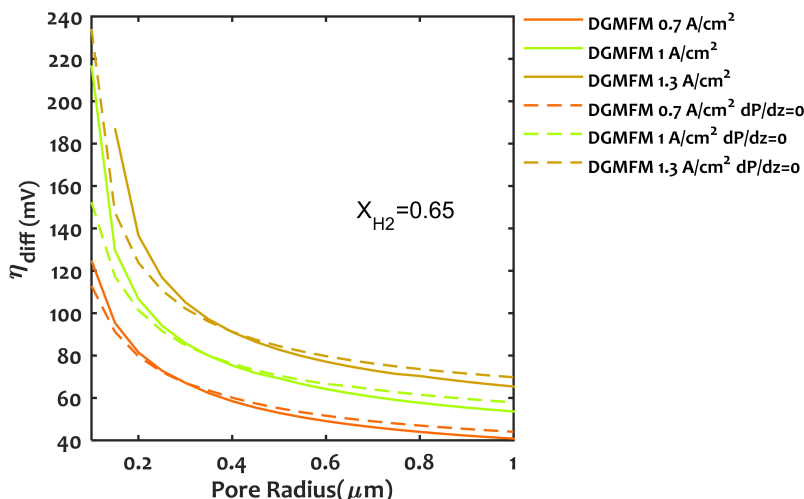


Figure 14. Comparison of diffusion overpotential predicted by the DGMFM with and without the pressure gradient for the ternary system.

The BFM and MBFM give similar predictions for the entire range of parameters applied.

Thus, the fractional viscosity coefficient for the modified binary friction model is unable to account for diffusive slip when the pressure gradient is ignored. At large pore radius, the current density increase does not have any major impact on the models' efficacy post pressure gradient term exclusion. The maximum difference remains below 10 mV for all the models. When the pore radius drops below 0.6 μm, the diffusion overpotential gets underestimated by 10–50 mV depending upon the current density and H₂ concentration. In Figure 14, the diffusion overpotential predicted by DGMFM with and without the pressure gradient inclusion is plotted. The range of pore radius is taken as 0.1–1 μm at moderate to high current density for a fixed H₂ mole fraction of 0.65. At large pore radius, exclusion of the pressure gradient term in DGMFM leads to an overestimation of diffusion overpotential by 2–4 mV. At small pore radius, the DGMFM underestimates the

diffusion overpotential by 2–20 mV. The DGMFM changes prediction trend right around the point where the number of wall molecule interactions increases rapidly. Hence, the pressure gradient term should not be excluded for DGMFM. In Figure 15 a graphical illustration on models' recommended implementation range along the SOFC's Cell Voltage (V) – Current Density (j) curve is presented. The factors considered include pore radius, pressure gradient and current density.

4. CONCLUSIONS

A one-dimensional modelling study on six different mass transfer models was conducted to compare their ability to predict the diffusion overpotential in SOFC anode. All the models were numerically solved for CO–CO₂ and H₂–H₂O–Ar systems. The results obtained were validated against experimental data acquired from the literature. The effects of pore radius, fuel concentration, current density and pressure gradient across anode were analyzed quantitatively over a broad range of parameters.

- The diffusion overpotential increases when fuel concentration or pore radius decrease. When the current density and pressure gradient are increased, the diffusion overpotential increases rapidly after a 0.6 μm pore radius lower threshold due to a substantial upsurge in the rate of wall molecule interaction.
- The exclusion of the extra flux term in DGMFM represented in Equation (25) leads to an erroneous evaluation of the fuel flux rate in SOFC anode. However, the error is too small and can be ignored. The DGMFM is the best alternative to the DGM for a binary system. The difference in diffusion differential prediction of both models remains below 1 mV (very small). For the ternary system, the difference grows beyond 30 mV (large) with decrease in pore radius or current density. Hence, for the multi-component system, it should be used at large pore radius.

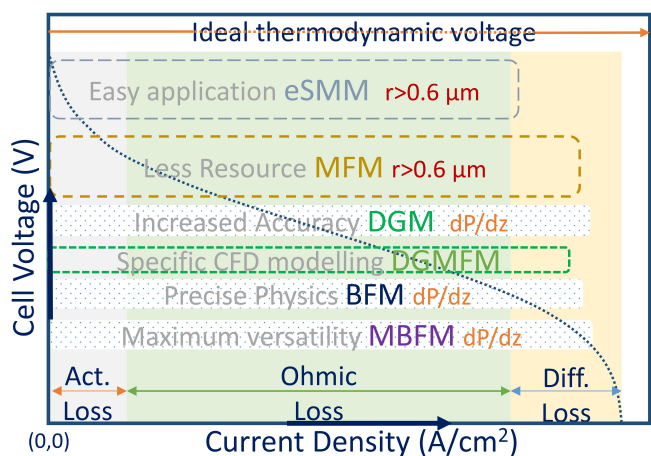


Figure 15. A graphical illustration on models' recommended implementation range along the SOFC's j–V curve.

- The MFM prediction remains very close to that of the DMG under experimental conditions and over a wider range of parameters. For the ternary system, the difference between the MFM and DGM avg. dev. remains below 0.2%. The MFM is a good replacement for the DGM for a large pore radius and up to medium current density for both systems. The difference in diffusion overpotential prediction of both models does not exceed 2 mV (small) for the entire range of parameters applied. As it turns out, the MFM is closer to the DGM than the DGMFM. It is better to choose the MFM instead of the DGMFM when the purpose is to get results closer to that of the DGM with independent flux equations.
- The empirical inclusion of the Knudsen diffusion coefficient in the eSMM leads to miscalculated fuel component flux rate. The eSMM does not offer a good agreement with the experimental data. Moreover, it is far from accurate beyond experimental conditions.
- Under the experimental conditions, the diffusive slip phenomenon inclusion in the MBFM creates a difference in avg. dev. below 0.5% and 1% against the BFM and DGM respectively. Further parametric comparison between the BFM and MBFM produced a maximum difference in diffusion over potential prediction below 5 mV (small). However, this very small difference is present in the SOFC anode due to difference in molecular mass of fuel components. For the ternary system, the diffusive slip effect is very small due to small size of fuel and product components. For the binary system, the MBFM deviates more due to increase in diffusive slip due to large CO and CO₂ molecules. It is clear that the diffusive slip phenomenon can play a role in SOFC mass transfer related losses when the fuel contains heavy molecules. Thus, the diffusive slip should not be ignored for hydrocarbon SOFC due to large size of fuel components with a significant difference in molecular mass.
- For the ternary system, the MBFM is a good alternative to the DGM as the difference in diffusion overpotential prediction of both models does not exceed 15 mV (small). For the binary system, this difference remains below 15 mV only for pore radius above 0.6 μm. If the small difference between the DGM and MBFM is adjusted using a tortuosity factor, the ability to account for the difference in molecular mass of fuel components makes the MBFM a good choice for hydrocarbon SOFC.
- At higher current density, all the described models fail to accurately predict the diffusion overpotential of SOFC. The avg. dev. rises above 80%. However, using these models in 3D may help better predict the diffusion overpotential of SOFC at higher current density.
- The pressure gradient term has a very small effect on diffusion overpotential calculation for the majority of H₂ and CO concentrations. For pore radius above 0.6 μm, as the current density increases, the maximum difference with and without the pressure gradient term remains below

10 mV for all the models. At low pore radius, the pressure gradient term should not be ignored as the difference can go beyond 50 mV. The DGMFM changes prediction trend when the number of wall molecule interactions increases rapidly. Therefore, the pressure gradient term should not be excluded for DGMFM.

ACKNOWLEDGEMENTS

The lead author would like to acknowledge the Department of Science and Technology, India for supporting the research work through a research fellowship.

SYMBOLS

1D	one dimensional system
Ar	argon molecule
B_0	permeability, m ²
CO	carbon monoxide molecule
CO ₂	carbon dioxide molecule
CH ₄	methane molecule
°C	degree centigrade
c_i	molar concentration of component, mol
D_i	equivalent diffusion coefficient
D_{ij}^{eff}	effective binary diffusion coefficient between gaseous species i and j
D_{iM}^{eff}	effective Knudsen diffusion coefficient for component i
e^-	electronic charge, Coulomb
F	Faraday constant
f_{im}	wall-friction coefficient of component i
H ₂	hydrogen molecule
H ₂ O	water molecule
j	current density, A/cm ²
K	Kelvin
k_i	equivalent permeability coefficient
k_b	Boltzmann constant
Kn	Knudsen number
l_a	length of anode, m
M_i	molecular mass of component i , g/mol or kg/mol
N ₂	nitrogen molecule
N_i	molar mass transport flux of component i , mol m ⁻² s ⁻¹
O ₂	oxygen molecule
O ²⁻	oxide ion
P	pressure, kPa
p_i	partial pressure of component i , kPa
Q	charge, Coulomb
R	universal gas constant
r_i	rate of reaction for component i
r, r_p	pore radius, m
T	temperature, K
t	time, s
V	specific fuller volume
x_i	mole fraction of component i
Z	axis direction

Greek symbols

κ_i	fractional viscosity coefficient
ε	porosity
τ^2	tortuosity factor
μ_i	component viscosity, Pa·s
μ	mixture viscosity, Pa·s
σ	collision diameter, Å
Ω_v	temperature dependent collision integral
ω	Lennard–Jones potential parameter
η_{diff}	diffusion overpotential
χ_i	modified fractional viscosity coefficient of component i

Subscripts

bulk	bulk
diff	diffusion
eff	effective
i, j	component
ref	reference

REFERENCES

- Abdalla A.M., Hossain S., Azad A.T., Petra P.M.I., Begum F., Eriksson S.G., Azad A.K., 2018. Nanomaterials for solid oxide fuel cells: A review. *Renewable Sustainable Energy Rev.*, 82, 353–368. DOI: [10.1016/J.RSER.2017.09.046](https://doi.org/10.1016/J.RSER.2017.09.046).
- Bao C., Jiang Z., Zhang X., 2016. Modeling mass transfer in solid oxide fuel cell anode: I. Comparison between Fickian, Stefan–Maxwell and dusty-gas models. *J. Power Sources*, 310, 32–40. DOI: [10.1016/j.jpowsour.2016.01.099](https://doi.org/10.1016/j.jpowsour.2016.01.099).
- Błesznowski M., Sikora M., Kupecki J., Makowski Ł., Or-ciuch W., 2022. Mathematical approaches to modelling the mass transfer process in solid oxide fuel cell anode. *Energy*, 239, 121878. DOI: [10.1016/j.energy.2021.121878](https://doi.org/10.1016/j.energy.2021.121878).
- Bove R., Ubertini S. (Eds.), 2008. *Modeling Solid Oxide Fuel Cells: Methods, Procedures and Techniques*. Springer Dordrecht. DOI: [10.1007/978-1-4020-6995-6](https://doi.org/10.1007/978-1-4020-6995-6).
- Cayan F.N., Pakalapati S.R., Elizalde-Blancas F., Celik I., 2009. On modeling multi-component diffusion inside the porous anode of solid oxide fuel cells using Fick's model. *J. Power Sources*, 192(2), 467–474. DOI: [10.1016/j.jpowsour.2009.03.026](https://doi.org/10.1016/j.jpowsour.2009.03.026).
- Chou Y.S., Hardy J., Marina O.A., 2022. Leak test for solid oxide fuel cells and solid oxide electrolysis cells. *Front. Energy Res.*, 10, 1459. DOI: [10.3389/fenrg.2022.945788](https://doi.org/10.3389/fenrg.2022.945788).
- Gholaminezhad I., Paydar M.H., Jafarpur K., Paydar S., 2017. Multi-scale mathematical modeling of methane-fueled SOFCs: Predicting limiting current density using a modified Fick's model. *Energy Convers. Manage.*, 148, 222–237. DOI: [10.1016/j.enconman.2017.05.071](https://doi.org/10.1016/j.enconman.2017.05.071).
- Haberman B.A., Young J.B., 2006. Diffusion and chemical reaction in the porous structures of Solid Oxide Fuel Cells. *J. Fuel Cell Sci. Technol.*, 3, 312–321. DOI: [10.1115/1.2211637](https://doi.org/10.1115/1.2211637).
- He W., Lv W., Dickerson J., 2014. *Gas transport in Solid Oxide Fuel Cells*. Springer Cham. DOI: [10.1007/978-3-319-09737-4](https://doi.org/10.1007/978-3-319-09737-4).
- Jacobson A.J., 2010. Materials for Solid Oxide Fuel Cells. *Chem. Mater.*, 22, 660–674. DOI: [10.1021/cm902640j](https://doi.org/10.1021/cm902640j).
- Kerkhof P.J.A.M., 1996. A modified Maxwell–Stefan model for transport through inert membranes: the binary friction model. *Chem. Eng. J. Biochem. Eng. J.*, 64, 319–343. DOI: [10.1016/S0923-0467\(96\)03134-X](https://doi.org/10.1016/S0923-0467(96)03134-X).
- Kong W., Gao X., Liu S., Su S., Chen D., 2014. Optimization of the interconnect ribs for a cathode-supported Solid Oxide Fuel Cell. *Energies*, 7, 295–313. DOI: [10.3390/en7010295](https://doi.org/10.3390/en7010295).
- Kong W., Zhu H., Fei Z., Lin Z., 2012. A modified dusty gas model in the form of a Fick's model for the prediction of multicomponent mass transport in a solid oxide fuel cell anode. *J. Power Sources*, 206, 171–178. DOI: [10.1016/j.jpowsour.2012.01.107](https://doi.org/10.1016/j.jpowsour.2012.01.107).
- Krishna R., Wesselingh J., 1997. The Maxwell–Stefan approach to mass transfer. *Chem. Eng. Sci.*, 52, 861–911. DOI: [10.1016/S0009-2509\(96\)00458-7](https://doi.org/10.1016/S0009-2509(96)00458-7).
- Lehnert W., Meusinger J., Thom F., 2000. Modelling of gas transport phenomena in SOFC anodes. *J. Power Sources*, 87, 57–63. DOI: [10.1016/S0378-7753\(99\)00356-0](https://doi.org/10.1016/S0378-7753(99)00356-0).
- Mason E.A., Malinauskas A.P., 1983. *Gas transport in porous media: The dusty-gas model*. Elsevier Scientific Pub. Co., Amsterdam, New York.
- Milewski J., Lewandowski J., 2011. Comparative analysis of time constants in Solid Oxide Fuel Cell processes – selection of key processes for modeling power systems. *J. Power Technol.*, 91(1), 1–5.
- Modjtahedi A., Hedayat N., Chuang S.S.C., 2016. Diffusion-limited electrochemical oxidation of H₂/CO on Ni-anode catalyst in a CH₄/CO₂-solid oxide fuel cell. *Catal. Today*, 278, 227–236. DOI: [10.1016/j.cattod.2015.12.026](https://doi.org/10.1016/j.cattod.2015.12.026).
- Neufeld P.D., Janzen A.R., Aziz R.A., 1972. Empirical equations to calculate 16 of the transport collision integrals $\Omega^{(l,s)*}$ for the Lennard–Jones (12-6) potential. *J. Chem. Phys.*, 57, 1100–1102. DOI: [10.1063/1.1678363](https://doi.org/10.1063/1.1678363).
- Ni M., Leung D.Y.C., Leung M.K.H., 2008. Importance of pressure gradient in solid oxide fuel cell electrodes for modeling study. *J. Power Sources*, 183, 668–673. DOI: [10.1016/j.jpowsour.2008.05.013](https://doi.org/10.1016/j.jpowsour.2008.05.013).
- O'Hayre R., Cha S.-W., Colella W., Prinz F.B. (2016). *Fuel Cell Fundamentals*. 3rd edition, Wiley, 206–207.
- Pant L.M., Mitra S.K., Secanell M., 2013. A generalized mathematical model to study gas transport in PEMFC porous media. *Int. J. Heat Mass Transfer*, 58, 70–79. DOI: [10.1016/j.ijheatmasstransfer.2012.11.023](https://doi.org/10.1016/j.ijheatmasstransfer.2012.11.023).
- Poling B., Prausnitz J., O'Connell J.P., 2000. *The properties of gases and liquids*. 5th edition. McGraw-Hill.
- Shaikh S.P.S., Muchtar A., Somalu M.R., 2015. A review on the selection of anode materials for solid-oxide fuel cells. *Renewable Sustainable Energy Rev.*, 51, 1–8. DOI: [10.1016/j.rser.2015.05.069](https://doi.org/10.1016/j.rser.2015.05.069).
- Singhal S.C., Kendall K., 2003. *High-temperature Solid Oxide Fuel Cells: Fundamentals, design and applications*. Elsevier. DOI: [10.1016/B978-1-85617-387-2.X5016-8](https://doi.org/10.1016/B978-1-85617-387-2.X5016-8).

- Suwanwarangkul R., Croiset E., Fowler M.W., Douglas P.L., Entchev E., Douglas M.A., 2003. Performance comparison of Fick's, dusty-gas and Stefan–Maxwell models to predict the concentration overpotential of a SOFC anode. *J. Power Sources*, 122, 9–18. DOI: [10.1016/S0378-7753\(02\)00724-3](https://doi.org/10.1016/S0378-7753(02)00724-3).
- Taylor R., Krishna R., 1993. *Multicomponent mass transfer*. John Wiley & Sons, Inc.
- Tseronis K., Kookos I.K., Theodoropoulos C., 2008. Modelling mass transport in solid oxide fuel cell anodes: a case for a multi-dimensional dusty gas-based model. *Chem. Eng. Sci.*, 63, 5626–5638. DOI: [10.1016/j.ces.2008.07.037](https://doi.org/10.1016/j.ces.2008.07.037).
- Vogler M., Bieberle-Hütter A., Gauckler L., Warnatz J., Bessler W.G., 2009. Modelling study of surface reactions, diffusion, and spillover at a Ni/YSZ patterned anode. *J. Electrochem. Soc.*, 156, B663. DOI: [10.1149/1.3095477](https://doi.org/10.1149/1.3095477).
- Vural Y., Ma L., Ingham D.B., Pourkashanian M., 2010. Comparison of the multicomponent mass transfer models for the prediction of the concentration overpotential for solid oxide fuel cell anodes. *J. Power Sources*, 195, 4893–4904. DOI: [10.1016/j.jpowsour.2010.01.033](https://doi.org/10.1016/j.jpowsour.2010.01.033).
- Wang S., Worek W.M., Minkowycz W.J., 2012. Performance comparison of the mass transfer models with internal reforming for solid oxide fuel cell anodes. *Int. J. Heat Mass Transfer*, 55, 3933–3945. DOI: [10.1016/j.ijheatmasstransfer.2012.03.024](https://doi.org/10.1016/j.ijheatmasstransfer.2012.03.024).
- Yakabe H., Hishinuma M., Uratani M., Matsuzaki Y., Yasuda I., 2000. Evaluation and modeling of performance of anode-supported solid oxide fuel cell. *J. Power Sources*, 86, 423–431. DOI: [10.1016/S0378-7753\(99\)00444-9](https://doi.org/10.1016/S0378-7753(99)00444-9).
- Yang F., Gu J., Ye L., Zhang Z., Rao G., Liang Y., Wen K., Zhao J., Goodenough J.B., He W., 2016. Justifying the significance of Knudsen diffusion in solid oxide fuel cells. *Energy*, 95, 242–246. DOI: [10.1016/j.energy.2015.12.022](https://doi.org/10.1016/j.energy.2015.12.022).
- Zhou W., Jiao Y., Li S.-D., Shao Z., 2016. Anodes for carbon-fueled Solid Oxide Fuel Cells. *ChemElectroChem*, 3, 193–203. DOI: [10.1002/celec.201500420](https://doi.org/10.1002/celec.201500420).
- Zhu H., Kee R.J., 2003. A general mathematical model for analyzing the performance of fuel-cell membrane-electrode assemblies. *J. Power Sources*, 117, 61–74. DOI: [10.1016/S0378-7753\(03\)00358-6](https://doi.org/10.1016/S0378-7753(03)00358-6).
- Zhu H., Kee R.J., Janardhanan V.M., Deutschmann O., Goodwin D.G., 2005. Modeling elementary heterogeneous chemistry and electrochemistry in Solid-Oxide Fuel Cells. *J. Electrochem. Soc.*, 152, A2427. DOI: [10.1149/1.2116607](https://doi.org/10.1149/1.2116607).